Catalysis Letters Vol. 112, Nos. 3–4, December 2006 (© 2006)
DOI: 10.1007/s10562-006-0194-8

Catalytic oxidation of diesel soot on mixed oxides derived from hydrotalcites

Zhongpeng Wang,[a] Wenfeng Shangguan,[a,*] Jixin Su,[b] and Zhi Jiang[a]

[a]*Research Center for Combustion and Environmental Technology, School of Mechanical and Power Engineering, Shanghai Jiao Tong University, Shanghai, 200030, P.R. China*

[b]*School of Environmental Science and Engineering, Shandong University, Jinan, 250100 Shandong Province, P.R. China*

Received 18 July 2006; accepted 5 October 2006

MAlO (where M = Ni^{2+}, Co^{2+} and Cu^{2+}) mixed oxides derived from hydrotalcites and potassium-promoted MAlO catalysts (designated as K/MAlO; K: 5 wt.%) have been studied for diesel soot oxidation. The catalysts were characterized by XRD, N_2 adsorption, TPR, FT-IR and TPO techniques. The hydrotalcites calcined at 800 °C have large surface areas in the range 17–88 m^2/g and uniform mesoporous features, which resulted in high activity for diesel soot oxidation under the conditions of tight contact between soot and catalyst powders. Potassium increased the activity due to the improvement of surface mobility. The presence of NO_x considerably enhanced the catalytic soot oxidation rate. The enhancement was attributed to the acceleration of soot oxidation due to NO_2 as a strong oxidizing agent and intermediates of nitrate and/or nitrite species formed on the catalyst surface.

KEY WORDS: Hydrotalcite; Mixed oxides; Diesel soot; Catalytic oxidation.

1. Introduction

Soot particulates and nitrogen oxides are the main pollutants in diesel engine emissions causing serious problems to global environment and human health. Many countries, such as U.S., Japan and Europe have introduced specific and severe limits to exhaust-gas emissions. Due to the more stringent legislation limitation, there is a growing interest in developing the process which enables the reduction of such emissions.

Soot emissions can be reduced by means of filtration within the exhaust stream. It is very important that the filter is robust and its regeneration is controllable. The key technology to controllable regeneration is oxidation catalysis [1]. Various materials have been studied as soot oxidation catalysts. Simple metal oxides, transition metal oxides and rare earth-based catalysts exhibited soot oxidation activity [2]. Perovskite-type oxides [3] and spinel-type oxides [4,5] showed good activities in simultaneous removal of NO_x and soot under lean conditions. Moreover, it has been concluded that the contact between soot and catalysts is a key factor in the catalytic soot oxidation [6].

On the other hand, hydrotalcite (HT) and Hydrotalcite-like compounds (HTlcs) are widely applied in catalysis and adsorption due to their changeable compositions and special structural properties. These materials can be chemically expressed by the formula $[M(II)_{1-x}M(III)_x(OH)_2]^{x+}[(A^{n-})_{x/n}\cdot mH_2O]^{x-}$, where M(II) represents any divalent metal cation, M(III) any trivalent metal cation, and A^{n-} an anion [7]. At higher temperatures hydrotalcites are transformed to mixed metal oxides, which are excellent catalysts or catalyst supports because of their large surface areas, basic properties, high metal dispersions and stability against sintering. In the last decade, the interests in application of HT-derived mixed oxides as environmental catalysts have significantly increased. Calcined hydrotalcites have been found to be active and selective catalysts of $DeNO_x$ with ammonia [8], as well as catalytic decomposition of NO and N_2O [9,10]. Such mixed oxides have been also employed as catalysts or catalyst support in redox reactions by incorporating transition metals, with redox properties, in the HT structure [11,12]. Their redox performances are strongly related to the metal species, contents and calcined temperatures. Copper-, cobalt- or nickel-based oxides derived from HT are known to be active catalysts for oxidation reactions [13,14].

In the present investigation, we report the use of Ni-, Co- and Cu-based oxides catalysts derived from hydrotalcites for diesel soot oxidation. The physicochemical properties of HT precursors and mixed oxides prepared by calcination are characterized by XRD, N_2 adsorption, TPR and FT-IR techniques. The catalytic activity tests for soot oxidation were carried out by the TPO experiments. The positive effects of potassium and NO on the catalytic activity were also discussed.

*To whom correspondence should be addressed.
E-mail: shangguan@sjtu.edu.cn

2. Experimental

2.1. Catalyst preparation

The synthesis of M(II)-Al HT (M = Ni, Co and Cu; M/Al molar ratio equals to 3) followed the reference [14] by co-precipitation of an aqueous solution of suitable metal nitrates with an aqueous solution of 2 M NaOH and 1 M Na_2CO_3. The two solutions were mixed under vigorous stirring at 25 °C and the pH was maintained constant at 10.0 ± 0.2. The resulting gel was aged in the mother liquor at 80 °C for 18 h. It was then filtered and washed with distilled water until the pH of the wash water became 7.0 and dried overnight at 100 °C. The obtained hydrotalcites precursors were calcined at 800 °C for 5 h in air. The catalysts were designated as MAlO.

The potassium-promoted catalysts (designated as K/MAlO, K: 5 wt.%) were prepared by impregnation of MAlO powder with an aqueous solution of K_2CO_3. The suspension was evaporated while being vigorously stirred until achieving a paste which was dried at 100 °C for 24 h and then calcined at 700 °C for 3 h.

2.2. Catalyst characterization

XRD was conducted with a BRUKER-AXS D8Adance X-Ray Diffractometer using Cu-Kα radiation, at 40 kV and 40 mA, in the scanning angle (2θ) range of 5°–80° at a scanning speed of 4°. N_2 adsorption/desorption isotherms were measured on a Quanta Chrome NOVA1000 Sorptomatic apparatus. The BET specific surface area (S_{BET}) was calculated by using the standard BET method on the basis of the adsorption data. Temperature-programmed reduction (TPR) analysis was carried out using a gas mixture of H_2–Ar (5 vol.%) and the gas flow (50 ml/min), sample weight (25 mg), and heating schedule (20 °C/min). H_2 consumption was measured using a thermal conductivity detector. Infrared spectra were obtained using a PE Paragn 1000 spectrometer. The samples were prepared in the form of pressed wafers (2% of sample in KBr).

2.3. Catalytic activity testing

In this paper, a commercially available carbon black (Shanxi Luan Carbon Black Science & Technology Co. Ltd, China) was used as model diesel soot. The catalytic activity tests for soot combustion were carried out by a Temperature-programmed oxidation (TPO) technique in a fixed-bed flow reactor under atmospheric pressure. Catalyst and soot (20:1 w/w) were well mixed by grinding for 10 min in an agate mortar, then the mixture was palletized (for 10 min under the pressure of 400 kg cm^{-2}), crushed and sieved to 20–40 mesh. The soot–catalyst mixture (0.5 g) was placed in an 8-mm U-shaped quartz reactor, and then pretreated in a helium flow at 300 °C for 2 h in order to eliminate possible contaminants. After cooling down the mixture to 100 °C and replacing the helium flow with the reaction gas flow, the same mixture was pretreated again for an hour. Then TPO was started at a heating rate of 1 °C/min. Two gas flow compositions were used: (1) 5 vol.% O_2 (80 cm^3/min) and (2) 0.25 vol.% NO + 5 vol.% O_2 (80 cm^3/min), the balance being helium. The outlet gas was analyzed with intervals of about 15 min using a TCD gas chromatograph (Shimazu GC-14B) with columns of molecular sieve 5A for CO_2 and N_2O and Porapak Q for separating N_2, O_2, NO and CO.

From TPO results, two parameters were derived in order to evaluate the catalytic performance: one is the ignition temperature of the soot (T_i) estimated by extrapolating the steeply ascending portion of the carbon dioxide formation curve to zero carbon dioxide concentration, and another is the peak temperature (T_p), namely, the one at maximum soot oxidation rate.

3. Results and discussion

3.1. X-ray diffraction analysis

The XRD patterns of M(II)-Al HT (M = Ni, Co and Cu) are given in figure 1. All the compounds showed the typical diffraction patterns of HT-like materials having layered structure with intercalated carbonate anions [11]. The most crystalline precursor is Ni-Al HT (figure 1a), exhibiting sharp and symmetric reflections for the basal (003), (006) and (009) planes, and broad and asymmetric reflections for the non-basal (012), (015) and (018) planes. The (110) and (113) reflections can also be clearly distinguished. The XRD patterns of Co/Al HT (figure 1b) and Cu/Al HT (figure 1c) also indicate the presence of HT-like phase while the crystallinity decreases. Several extra peaks are found in the XRD pattern for Cu/Al HT, which might be assigned to malachite phase, being known to form in Cu/Al HT, especially at high Cu/Al ratios [15]. These results indicated that Ni^{2+}, Co^{2+} and Cu^{2+} were incorporated into the HT structures and the former two cations were well dispersed.

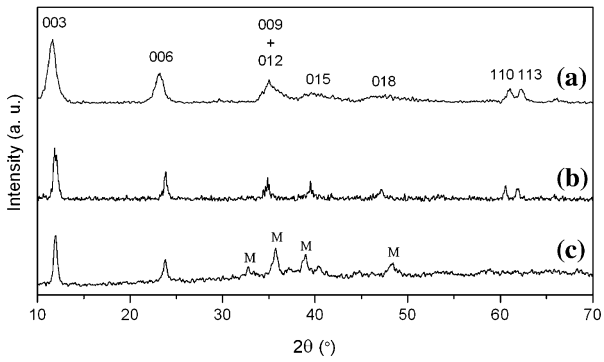

Figure 1. XRD patterns of M(II)-Al HT samples. (a) Ni/Al HT, (b) Co/Al HT, and (c) Cu/Al HT. (M): denoted to malachite $Cu(OH)_2$ phases.

The XRD patterns of calcined catalysts MAlO and K/MAlO are shown in figure 2. Different oxide phases were formed by calcining HT precursors. As previously reported [16], NiO phase was identified after thermal decomposition of Ni/Al HT. The Al^{3+} ions can either be incorporated in a separate amorphous phase, or in an amorphous nickel aluminate phase. In case of the CoAlO sample, reflections can be assigned to $CoAl_2O_4$ and Co_3O_4 spinel phases that are indistinguishable due to the similar reflection angles and intensities in XRD. As for CuAlO sample, CuO phase together with traces of $CuAl_2O_4$ spinel phase are detected in the XRD patterns. It can be seen from figure 2b that K/MAlO samples exhibit the same reflections as their MAlO supports and no other phases are detected. This means high dispersion of potassium species on the surface, which has been also observed in potassium-salt modified HT by Wang *et al.* [17].

3.2. N_2 adsorption/desorption characterization of MAlO and K/MAlO

Figure 3 compares N_2 adsorption/desorption isotherms of MAlO and K/MAlO. All samples show Type-IV isotherms with a H_3 hysteresis loop at a high relative pressure. This suggests that the catalyst has a broad pore size distribution in "large" mesoporous region, and almost without micropores [18]. From the nature of the loop, it can be concluded that the pores of MAlO and the corresponding potassium-promoted MAlO are of uniform shape. The BET specific surface area (S_{BET}), Total Pore Volume (V_P) and Average Pore Diameter (D_P) of the calcined samples determined from these isotherms are summarized in table 1. NiAlO sample showed the highest surface area (88.6 $m^2\ g^{-1}$) while it decreased to 57.9 $m^2\ g^{-1}$ when potassium was impregnated, namely K/NiAlO. The V_P also decreased markedly from 0.265 $cm^3\ g^{-1}$ to 0.124 $cm^3\ g^{-1}$, while D_P decreased from 12 nm to 8.5 nm. However, the three textural parameters of Co- or Cu-based catalysts did not change so greatly, which indicates a similarity in the porous structure of the samples before and after impregnation. CoAlO and CuAlO may be better supports for highly dispersed potassium than NiAlO.

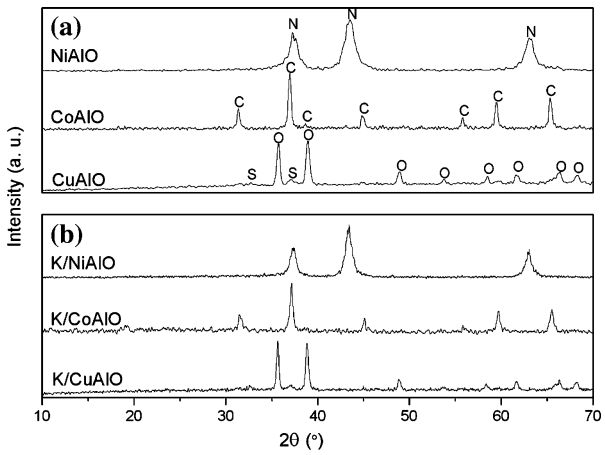

Figure 2. XRD patterns of MAlO (a) and K/MAlO samples (b). Crystalline phases identified as indicated: N-NiO, C-Cobalt spinel, O-CuO, S-$CuAl_2O_4$.

3.3. TPR results

TPR was used to examine the redox properties of catalysts. Figure 4 gives TPR data for MAlO and K/MAlO catalysts. The TPR patterns for the Ni-based catalysts exhibit a small and broad peak at 350–540 °C, which is due to reduction of Ni in the NiO phase. A much larger and broader peak is observed at 550–900 °C, suggesting the reduction of spinel phase ($NiAl_2O_4$) [11]. The spinel phase was not observed in the XRD results, which may be due to the high disperse of spinel. The hydrogen consumption for K/NiAlO (figure 4d) increased indicating that potassium can enhance the reduction of Ni^{2+} both in the NiO phase and in the lattice of spinel.

In the case of Co-based catalysts, TPR also displays two reduction regions, one between 300 °C and 500 °C and the other above 600 °C. The reduction at lower temperature can be attributed to the reduction of the Co_3O_4 spinel and well-dispersed surface Co^{3+} ions [19]. The other reduction peak can be assigned to the reduction of Co^{2+}–Al^{3+} like species, which behaves chemically like $CoAl_2O_4$ spinel [20]. The TPR results are in agreement with the XRD results where we observed the presence of $CoAl_2O_4$ and Co_3O_4 spinel phases. It is also shown that there is no remarkable change in hydrogen consumption for CoAlO and K/CoAlO.

The Cu-based catalysts exhibit the lowest reduction temperature among all samples. The reduction stage is mainly in the low-temperature range of 200–500 °C. In the TPR pattern of CuAlO (figure 4c), the large peak at around 385 °C is related to the reduction of Cu^{2+} cations in the CuO while the weak peak around 470 °C is probably due to the reduction of surface $CuAl_2O_4$ spinel [11]. This is in very good agreement with the XRD results that indicated the presence of CuO and $CuAl_2O_4$. For the K/CuAlO sample, the two peaks overlapped and the temperature for maximum rate of H_2 consumption shifted to 480 °C. Two small TPR peaks appeared at higher temperature attributed to the reduction of copper in spinel phase. This may be related to the transformation of CuO phase into spinel or promotion of reduction of Cu^{2+} in spinel after potassium impregnation.

3.4. FT-IR characterization

Figure 5 presents the FT-IR spectra of MAlO, K/MAlO (fresh solids), and $MAlO_{nt}$, $K/MAlO_{nt}$ (catalysts after NO + O_2 treatment at 100 °C for an hour). Mixed oxides derived from HT are known to be very sensitive

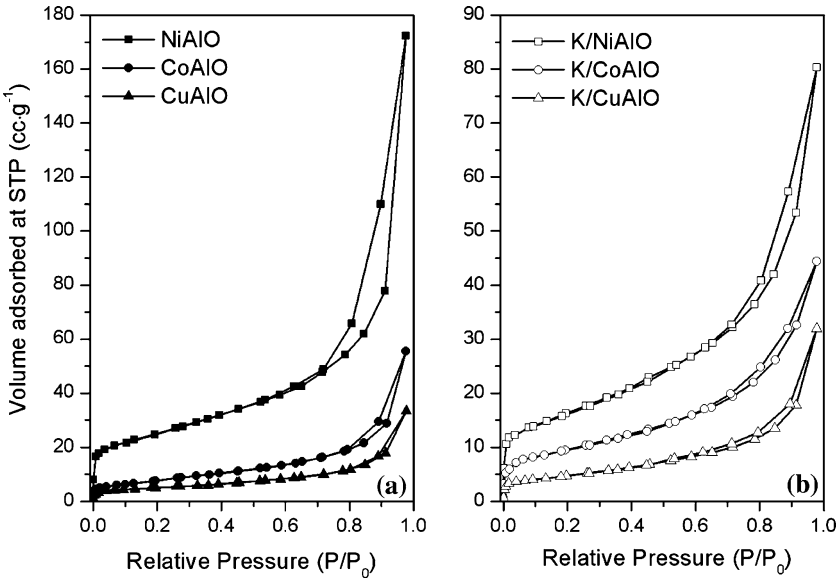

Figure 3. Nitrogen adsorption/desorption isotherm of MAlO (a) and K/MAlO (b) samples.

Table 1
Characteristics of the porous structure of the MAlO and K/MAlO

Sample	S_{BET} ($m^2\ g^{-1}$)	V_P ($cm^3\ g^{-1}$)	D_P (nm)
NiAlO	88.6	0.265	12.0
CoAlO	35.0	0.104	11.9
CuAlO	17.8	0.052	11.5
K/NiAlO	57.9	0.124	8.5
K/CoAlO	33.9	0.068	8.1
K/CuAlO	17.0	0.049	11.6

S_{BET} – BET specific surface area.
V_P – Total pore volume.
D_P – Average pore diameter.

to water and carbon dioxide exposure. For all samples, the absorption band centered around 1636 cm^{-1} can be attributed to the stretching mode of hydrogen-bonded hydroxyl groups of physically absorbed water on the oxide surfaces, while the weak broad band around 1000 cm^{-1} and another at 830 cm^{-1} correspond respectively to v_1 and v_2 vibrations mode of carbonate [21]. The remaining bands below 1000 cm^{-1} are most probably due to metal oxygen vibrations.

Figure 5a shows the FT-IR results of Ni-containing samples. Fresh solids (NiAlO and K/NiAlO) show a broad band around 1385 cm^{-1} which can be attributed to v_3 asymmetric stretching vibration of carbonate or nitrate [22]. As for $NiAlO_{nt}$ and $K/NiAlO_{nt}$, the band around 1385 cm^{-1} becomes sharper and a new band at 1270 cm^{-1} appears. The absorption changes at 1270 and 1385 cm^{-1} can be ascribed to the presence of unidentate ($-ONO_2$) and free nitrates (NO_3^-) anions [22], respectively. However, the former adsorption (1270 cm^{-1}) can be also attributed to the presence of surface nitrite (NO_2^-) anions [8]. These nitrate and/or nitrite species

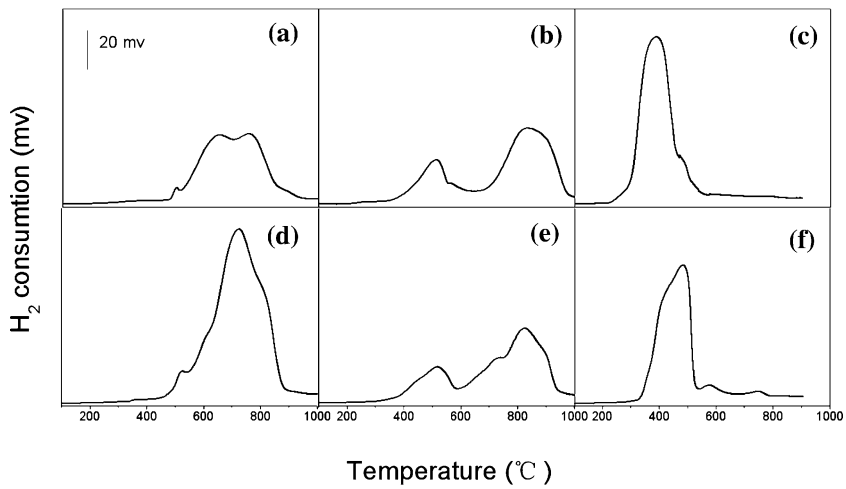

Figure 4. TPR patterns of samples. (a) NiAlO, (b) CoAlO, (c) CuAlO, (d) K/NiAlO, (e) K/CoAlO, and (f) K/CuAlO.

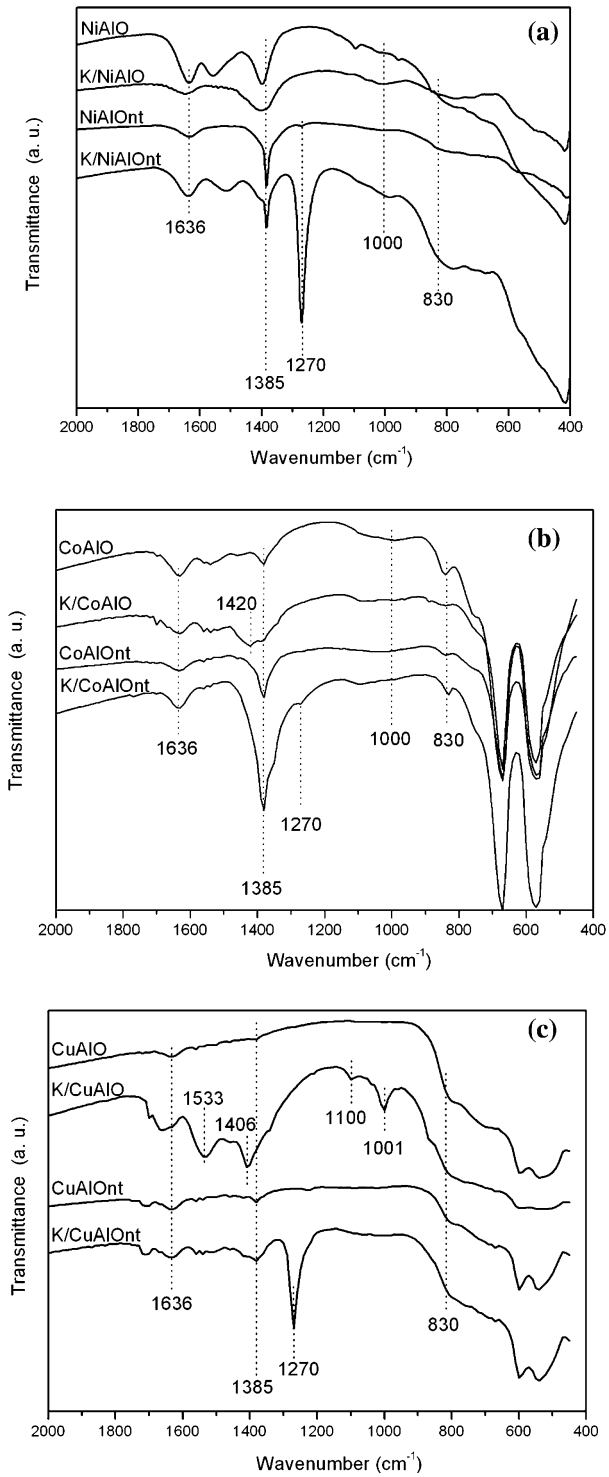

Figure 5. Infrared spectra of MAlO and K/MAlO samples. MAlO and K/MAlO: fresh samples; $MAlO_{nt}$ and $K/MAlO_{nt}$: catalysts after NO + O_2 treatment at 100 °C.

formed after NO + O_2 treatment may play an important role in the soot oxidation reaction.

The appearance of band at 1420 cm^{-1} in $K/CoAlO_{nt}$ (figure 5b) corresponds to the O–C–O vibrations in carbonate on the surface of the sample [23]. It seems to be associated with the highly dispersed potassium carbonate on the mixed oxides, which has been observed in the XRD results. Similar to Ni-containing samples, the band around 1385 cm^{-1} becomes sharper for both $CoAlO_{nt}$ and $K/CoAlO_{nt}$. The $K/CoAlO_{nt}$ sample also shows a weak shoulder at 1270 cm^{-1}, which proves that nitrate and/or nitrite species are also formed after NO + O_2 treatment. These features are also observed in the FT-IR spectra of the Cu-containing samples as shown in figure 5c. For fresh solids, CuAlO shows very weak vibrations of carbonate between 1600 and 1400 cm^{-1}, while K/CuAlO shows obvious CO_3^{2-} anion vibrations at 1533, 1406, 1100, and 1001 cm^{-1} in relation to potassium carbonate impregnation. The sharper bands at 1385 cm^{-1} for $CuAlO_{nt}$, and 1270 and 1385 cm^{-1} for $K/CuAlO_{nt}$ correspond to NO_x^- species formed on the surface of the solids after NO + O_2 treatment. In contrast with $K/CoAlO_{nt}$, the absorption at 1270 $cm^{-1}$for $K/NiAlO_{nt}$ and $K/CuAlO_{nt}$ are stronger.

3.5. Catalytic performance of diesel soot oxidation

The catalytic performances are compared by analyzing the TPO profiles (figure 6). NO CO was detected during the TPO process and the carbon mass balance was nearly 100 ± 5%.

As can be seen from figure 6a, the TPO profiles are very broad in the reaction gas of O_2/He. The non-catalytic soot oxidation begins at about 530 °C. In the case without promoted K, all of the ignition temperatures (T_i) for MAlO (M = Ni, Co and Cu) are about 320 °C and the combustion completes at about 600 °C. However, for the potassium promoted solids, both T_i and T_p shift to lower temperatures. For an example, the T_i and T_p of Co-based catalysts decrease to 269 °C and 350 °C from 316 °C and 430 °C respectively, due to the promoting effect of potassium. The promoting effect on soot oxidation is contributed to the increase of surface mobility by loading potassium, improving the contact between solid catalyst and solid soot [24].

In the presence of NO + O_2 (figure 6b), the TPO profiles become narrower and sharper. K/CuAlO sample shows the best soot oxidation activity with T_i = 251 °C and T_p = 350 °C, and the combustion completes at about 400 °C in the presence of NO + O_2. In soot–NO–O_2 system, the importance of NO_2 is well known [5]. Even at low temperature, NO can be readily oxidized to NO_2. It has been approved that the oxidizing ability of NO_2 is stronger than NO and O_2. The maximum oxidation rate for soot is considerably increased to about 300 $\mu g\ g^{-1}\ s^{-1}$ in the presence of NO, while it is about 150 $\mu g\ g^{-1}\ s^{-1}$ in the case without NO. FT-IR results shown in figure 5 have showed the adsorption of NO on the catalyst surface. It seems that the formed nitrate and/or nitrite species in soot–NO–O_2 reactions result in the positive influence on the activity. It has been also reported that the nitrate and/or nitrite are strong oxidizers and contribute to the oxidation of soot [25]. In

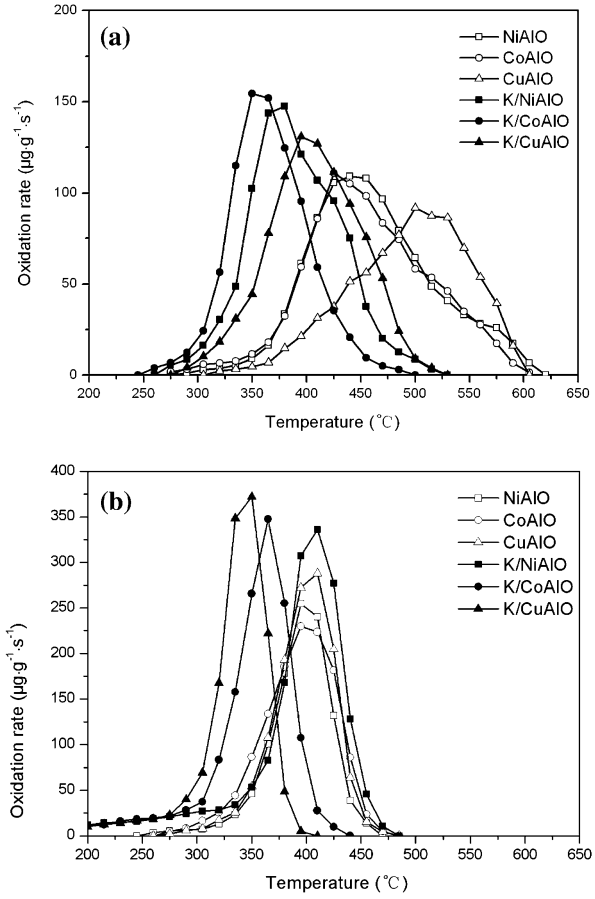

Figure 6. TPO results of soot catalyzed oxidation. Gas composition: (a) 5 vol.% O_2/He, (b) 0.25 vol.% NO + 5 vol.% O_2/He. Flow rate: 80 cm^3 min^{-1}.

this study, N_2 and/or N_2O were detected in the TPO process of all catalysts, which indicated that NO_x^- species took part in the soot oxidation reaction.

4. Conclusions

Mixed oxides MAlO (where M = Ni^{2+}, Co^{2+} and Cu^{2+}) can be derived from calcined binary hydrotalcites with M^{2+}/Al^{3+} atomic ratio 3. Ni^{2+} and Co^{2+} were well dispersed in hydrotalcites precursors, while a mixture of HT-like and malachite phase was formed for Cu/Al HT. Calcination of the hydrotalcites at 800 °C resulted in the formation of mixed oxides and spinels. K/MAlO samples prepared by impregnation method using K_2CO_3 exhibited uniform pore shapes with MAlO supports. Potassium carbonates were highly dispersed on MAlO samples. After NO + O_2 treatment, new nitrate and/or nitrite species were formed on MAlO and K/MAlO catalysts surface.

MAlO and K/MAlO catalysts were active for the oxidation of diesel soot into CO_2. Potassium increased the activity probably due to the improvement of surface mobility. The presence of NO_x in the reaction gas not only decreased the soot combustion temperatures, but also considerably increased the catalytic soot oxidation rate. The promotion effect is contributable to NO_2 as a strong oxidizing agent and nitrate and/or nitrite species formed in soot–NO–O_2 reactions.

Acknowledgments

This work was carried out with the financial support of GM-China Scientific Research Foundation (50222203). The authors are grateful to Prof. Y. Teraoka and Mr. H. Furukawa for their help in analytical apparatus.

References

[1] B.A.A.L. van Setten, M. Makkee and J.A. Moulijn, Catal. Rev. 43 (2001) 489.
[2] J.P.A. Neeft, M. Makkee and J.A. Moulijn, Chem. Eng. J. 64 (1996) 295.
[3] Y. Teraoka, K. Nakano, W. Shangguan and S. Kagawa, Catal. Today 27 (1996) 107.
[4] W.F. Shangguan, Y. Teraoka and S. Kagawa, Appl. Catal. B 8 (1996) 220.
[5] W.F. Shangguan, Y. Teraoka and S. Kagawa, Appl. Catal. B 12 (1997) 237.
[6] J.P.A. Neeft, M. Makkee and J.A. Moulijn, Appl. Catal. B 8 (1996) 57.
[7] A. Vaccari, Catal. Today 41 (1998) 53.
[8] L. Chmielarz, P. Kustrowski, A. Rafalska-Lasocha, D. Majda and R. Dziembaj, Appl. Catal. B 35 (2002) 195.
[9] A. Corma, A.E. Palomares, F. Rey and F. Marquez, J. Catal. 170 (1997) 140.
[10] S. Kannan, Appl. Clay Sci. 13 (1998) 347.
[11] L. Chmielarz, P. Kustrowski, A. Rafalska-Lasocha and R. Dziembaj, Thermochim. Acta 395 (2003) 225.
[12] J.J. Yu, Z. Jiang, L. Zhu, Z.P. Hao and Z.P. Xu, J. Phys. Chem. B 110 (2006) 4291.
[13] S. Velu, K. Suzuki and T. Osaki, Catal. Lett. 69 (2000) 43.
[14] Z. Jiang, Z.P. Hao, J.J. Yu, H.X. Hou, C. Hu and J.X. Su, Catal. Lett. 99 (2005) 157.
[15] Y. Lwin, M.A. Yarmo, Z. Yaakob, A.B. Mohamad and W.R.W. Daud, Mater. Res. Bull. 36 (2001) 193.
[16] S. Velu, K. Suzuki, M.P. Kapoor, S. Tomura, F. Ohashi and T. Osaki, Chem. Mater. 12 (2000) 719.
[17] Y. Wang, X.W. Han, A. Ji, L.Y. Shi and S. Hayashi, Micropor. Mesopor. Mater. 77 (2005) 139.
[18] M. Bolognini, F. Cavani, D. Scagliarini, C. Flego, C. Perego and M. Saba, Micropor. Mesopor. Mater. 66 (2003) 77.
[19] P.G. Harrison, I.K. Ball, W. Daniell, P. Lukinskas, M. Cespedes, E.E. Miro and M.A. Ulla, Chem. Eng. J. 95 (2003) 47.
[20] S. Velu, K. Suzuki and T. Osaki, Catal. Lett. 69 (2000) 43.
[21] F. Li, L.H. Zhang, D.G. Evans and X. Duan, Colloids Surf. A 244 (2004) 169.
[22] V.G. Milt, M.A. Ulla and E.E. Miro, Appl. Catal. B 57 (2005) 13.
[23] M.A. Aramendia, Y. Aviles, J.A. Benitez, V. Borau, C. Jimenez, J.M. Marinas, J.R. Ruiz and F.J. Urbano, Micropor. Mesopor. Mater. 29 (1999) 319.
[24] C.A. Querini, L.M. Cornaglia, M.A. Ulla and E.E. Miro, Appl. Catal. B 20 (1999) 165.
[25] V.G. Milt, C.A. Querini, E.E. Miro and M.A. Ulla, J. Catal. 220 (2003) 424.